Supplementary Information.

Single-particle structure determination by correlations of snapshot X-ray diffraction patterns

D. Starodub[1], A. Aquila[2,3,4], S. Bajt[4], M. Barthelmess[4], A. Barty[2], C. Bostedt[5], J.D. Bozek[5], N. Coppola[3], R.B. Doak[6], S.W. Epp[7,8], B. Erk[7,8], L. Foucar[9,7], L. Gumprecht[2], C.Y. Hampton[1], A. Hartmann[10], R. Hartmann[10], P. Holl[10], S. Kassemeyer[9], N. Kimmel[11,12], H. Laksmono[1], M. Liang[2], N.D. Loh[1], L. Lomb[9,7], A.V. Martin[2], K. Nass[2,13], C. Reich[10], D. Rolles[7,9], B. Rudek[7,8], A. Rudenko[7,8], J. Schulz[2], R.L. Shoeman[9], R.G. Sierra[1], H. Soltau[10], J. Steinbrener[9,7], F. Stellato[2], S. Stern[2], G. Weidenspointner[11,12], M. Frank[14], J. Ullrich[7,8,15], L. Strüder[11,12], I. Schlichting[9,7], H.N. Chapman[2,13], J.C.H. Spence[6], M.J. Bogan[1]

[1]PULSE Institute, SLAC National Accelerator Laboratory, 2575 Sand Hill Road, Menlo Park, CA 94025, USA,

[2]Center for Free-Electron Laser Science, DESY, Notkestrasse 85, 22607 Hamburg, Germany,

[3]European XFEL GmbH, Albert Einstein Ring 19, 22761 Hamburg, Germany,

[4]Photon Science, DESY, Notkestrasse 85, 22607 Hamburg, Germany,

[5]LCLS, SLAC National Accelerator Laboratory, 2575 Sand Hill Road, Menlo Park, CA 94025, USA,

[6]Department of Physics, Arizona State University, PO Box 871504, Tempe, AZ 85287, USA

[7]Max Planck Advanced Study Group, Center for Free Electron Laser Science (CFEL), Notkestrasse 85, 22607 Hamburg, Germany,

[8]Max-Planck-Institut für Kernphysik, Saupfercheckweg 1, 69117 Heidelberg, Germany,

[9]Max-Planck-Institut für medizinische Forschung, Jahnstr. 29, 69120 Heidelberg, Germany,

[10]PNSensor GmbH, Otto-Hahn-Ring 6, 81739 München, Germany,

[11]Max-Planck-Institut Halbleiterlabor, Otto-Hahn-Ring 6, 81739 München, Germany,

[12]Max-Planck-Institut für extraterrestrische Physik, Giessenbachstrasse, 85741 Garching, Germany,

[13]University of Hamburg, Luruper Chaussee 149, 22761 Hamburg, Germany,

[14]Lawrence Livermore National Laboratory, 7000 East Avenue, Livermore, CA 94550, USA,

[15]Physikalisch-Technische Bundesanstalt, Bundesallee 100, D-38116, Braunschweig, Germany.

Supplementary figures

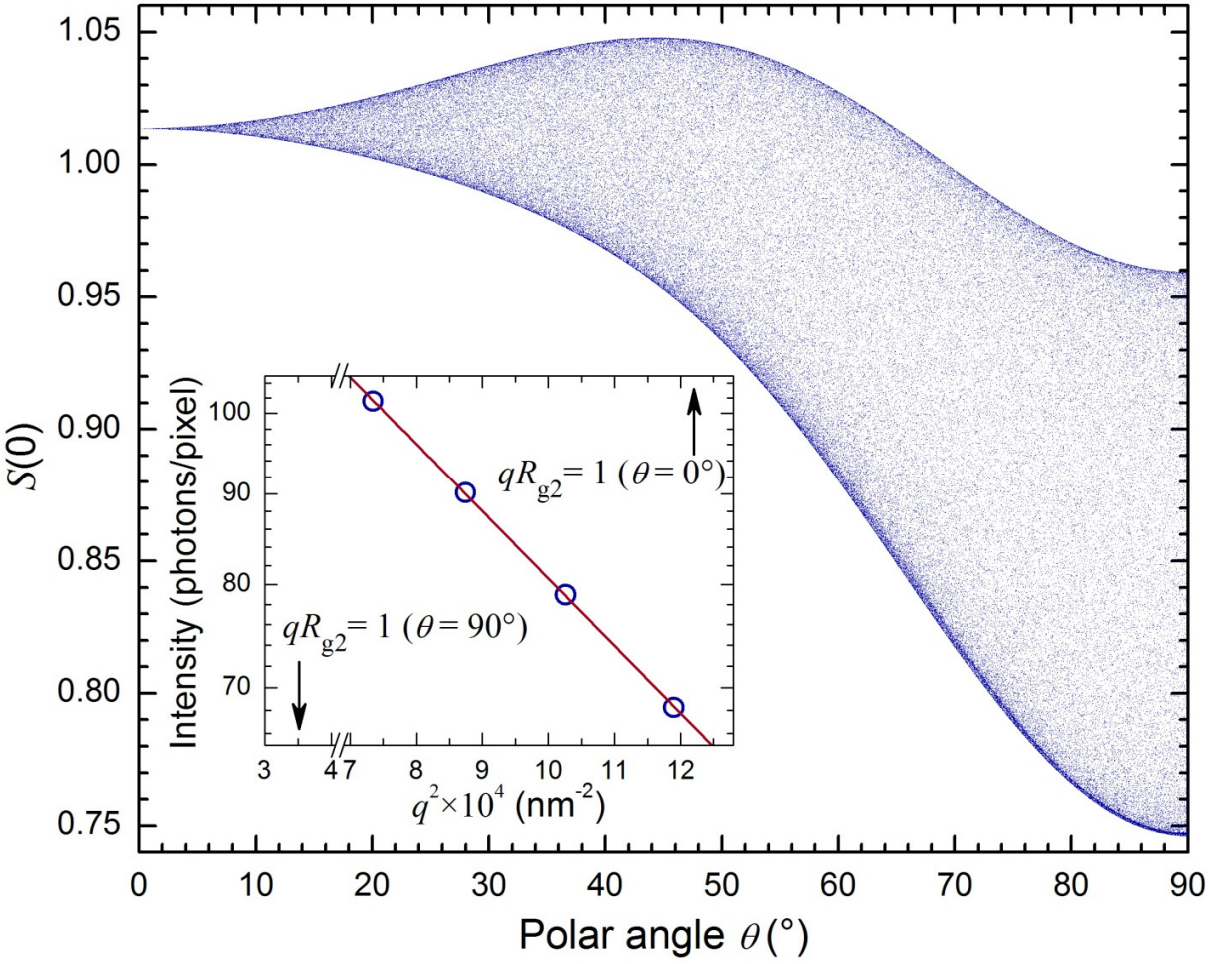

Supplementary Figure S1: Determination of the incident X-ray fluence. Measured normalized X-ray fluence for simulated diffraction patterns as a function of angle between direction of X-ray beam and axis of particle cylindrical symmetry. Inset shows a typical fit of the low-q experimental data (open circles) by straight line. This fit is valid in the q range to the left from the two arrows, corresponding to the orientation parallel and perpendicular to the X-ray beam.

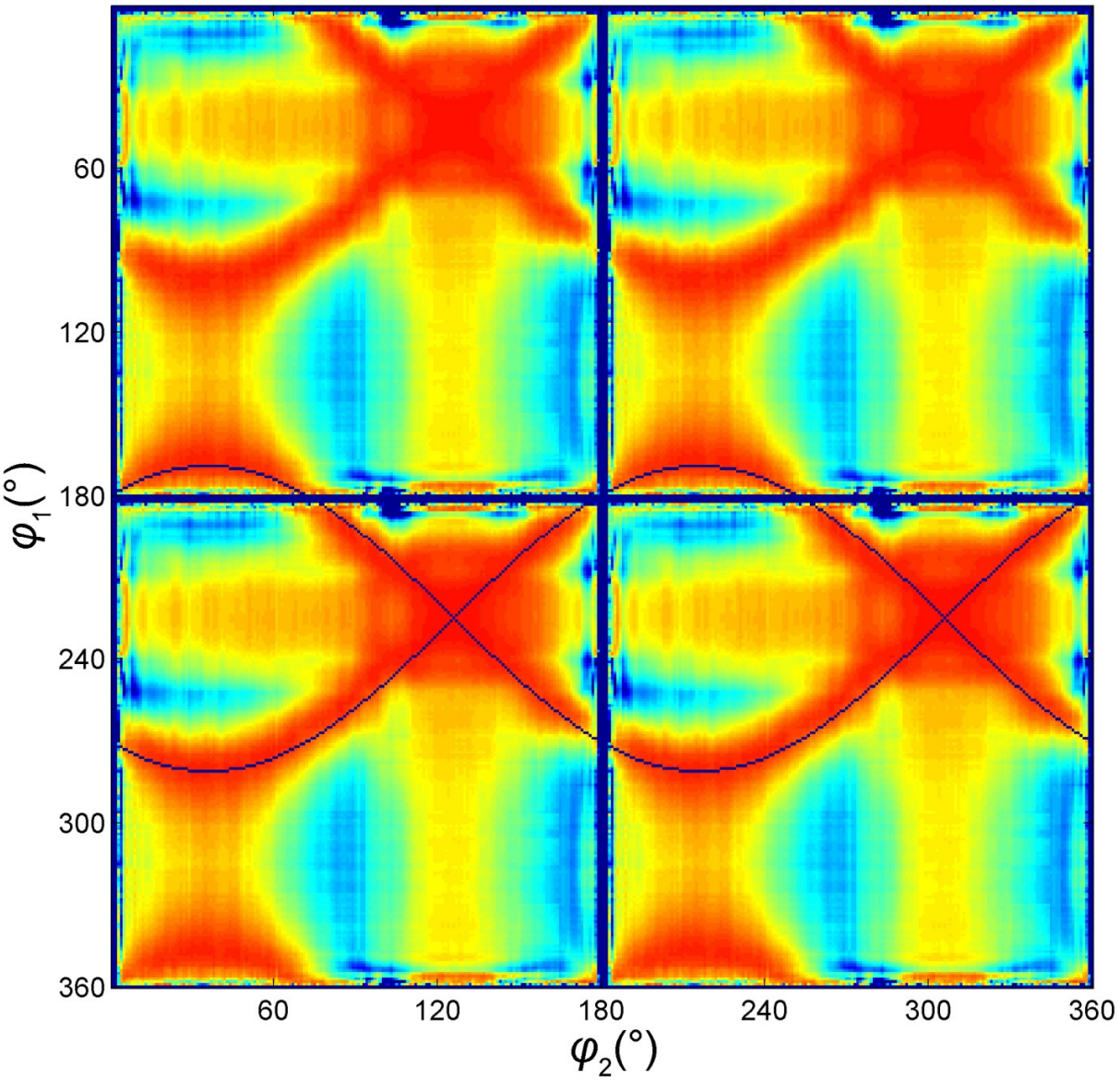

Supplementary Figure S2: Sinogram cross-correlation function for two diffraction patterns. Solid lines indicate its maxima, which identify the polar angles of the line common to both patterns. Empty and distorted regions in the vicinity of 0 and 180° are due to the gap between two detector halves.

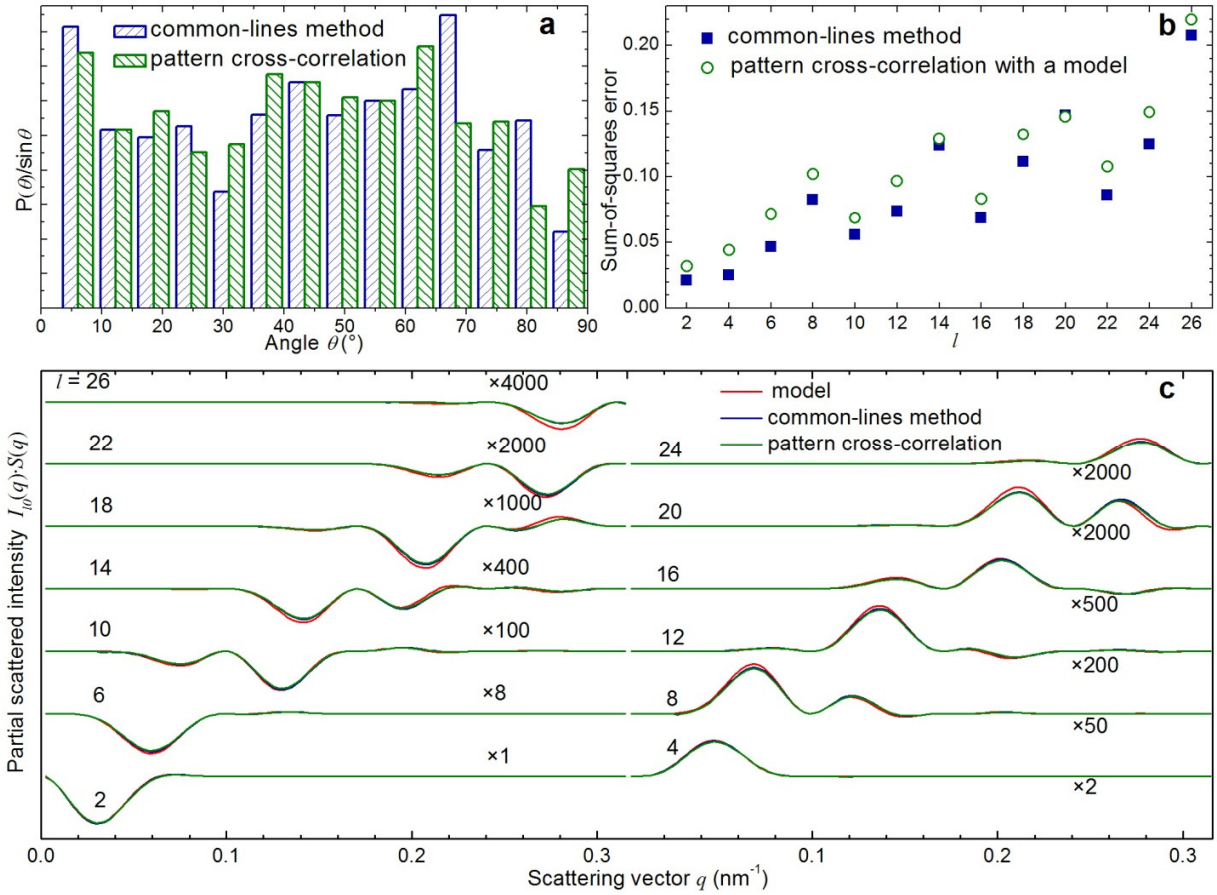

Supplementary Figure S3: Effect of particle orientation distribution on computation of partial scattered intensities. (**a**) Histograms of probability density for the polar angle θ calculated using the common-lines method and cross-correlation function between experimental and model diffraction patterns. (**b**) Square root of the sum-of-squares error between partial scattered intensities of degree l (indicated in horizontal axis) computed directly from the ideal particle shape and from simulated data sets with experimental orientations calculated by the respective methods. These partial scattered intensities are plotted in (**c**).

Supplementary Methods

X-ray fluence and particle orientation distributions. In principle, the incident X-ray fluence and dimer orientation can be derived from the integral properties of diffraction patterns. Similar to Guinier equation[30] for the spherically averaged scattered intensity, for the radially averaged 2D diffraction pattern from an individual particle at small values of scattering vector q we have $S(q) = S(0)\exp\left(-R_{g2}^2 q^2/2\right)$, where R_{g2} is the gyration radius about X-ray direction, and $S(0)$ is proportional to the incident X-ray fluence. The dimer gyration radius is determined by its orientation, defined by the angle θ between the axis of cylindrical symmetry and the X-ray direction. From the simple geometric consideration $\cos\theta = (7/5 - 2k/R^2)^{1/2}$, where R is the sphere's radius, and k the slope of the Guinier plot of $\ln S$ as a function of q^2. Depending on dimer orientation, its gyration radius R_{g2} varies between $\sqrt{2/5}\,R$ and $\sqrt{7/5}\,R$ for the dimer aligned with and perpendicular to the X-ray beam, respectively. Since Guinier approximation is only valid for $R_{g2}q < 1$, following this approach for the measured $q > 0.027$ nm^{-1} we were able to reliably determine X-ray fluence and particle orientation only for $\theta < 45°$. To estimate the error due to the missing data at low q, we computed $S(0)$ using Guinier plots in the experimentally available q range for a set of simulated diffraction patterns from dimers in uniformly distributed random orientations. The resultant X-ray fluence normalized to its actual value is plotted in Supplementary Fig. S1. The error in determination of fluence remains within 5% for $\theta < 45°$, and reaches as high as 25% for the particles oriented perpendicular to the X-ray beam.

To extend the range of validity of orientation determination, we used two other approaches. In the first method, we computed a set of central sections through a simulated dimer diffraction volume for the polar angle θ in the range between 0 and 90° with a step of 1°. For each experimental pattern the angular cross-correlation function between this pattern and each simulated pattern was computed. The orientation of the simulated pattern, for which this function has a maximum, was assigned to this experimental pattern. The second method involved common-lines search[16] in the experimental patterns. A sinogram cross-correlation function for two diffraction patterns extended for better visualization to the 360° range is given in Supplementary Fig. S2. Each row corresponds to the cross-correlation between one central line of the first pattern and all central lines of the second pattern. Instead of the peaks observed in general case, our sinogram cross-correlation function exhibits two continuous lines of maxima due to the sample symmetry leading to undefined azimuthal angle of the patterns. Their intersection gives the angles of the shared central line in the plane normal to the rotational symmetry axis, and distance between these lines reaches the maximum at 90° from intersection. To simplify the problem, we chose a high signal diffraction pattern through the axis of cylindrical symmetry as a reference central section. Then the polar angle θ for any other pattern can be found as a half of the maximum distance between the lines of maxima in the sinogram cross-correlation

function. Both methods gave mostly well-matched particle orientations with square root of sum-of-square error between them of 0.075. The corresponding probability densities for the orientation angle θ normalized by $\sin\theta$ are compared in the histograms in Supplementary Fig. S3a. Deviation of these functions from a straight horizontal line indicates that orientation distribution is not truly uniform. To estimate the bias introduced specifically by the non-uniformity of the measured orientation distribution, we generated two sets of 635 noise-free diffraction patterns with orientations obtained by common-lines method and cross-correlations with model central sections, respectively. The partial scattered intensities $I_{l0,exp}(q)$ were computed from these data and compared against the true values $I_{l0,mod}(q)$ calculated directly from the dumbbell particle shape as discussed in the next section. The results are plotted in Supplementary Fig. S3c. The sum-of-squares error

$$R = \left[\sum_q \left(I_{l0,exp}(q) - I_{l0,mod}(q)\right)^2 / \sum_q I_{l0,mod}^2(q)\right]^{1/2} \quad \text{(S1)}$$

for each l is shown in Supplementary Fig. S3b. We conclude from this analysis that deviations from the uniform orientation distribution found in our experiment did not significantly affect the partial scattered intensities derived in this work.

Spherical harmonics expansion of a dimer diffraction pattern. Partial scattering amplitude can be evaluated from particle electron density $\rho(\mathbf{r})$ as

$$A_{lm}(q) = \sqrt{2/\pi}\, i^l \int \rho(\mathbf{r})\, j_l(qr) Y_{lm}^*(\omega) d\mathbf{r}. \quad \text{(S2)}$$

Here $j_l(x)$ are spherical Bessel functions. Normalized density of a dimer composed of two touching spheres of radius a is given by

$$\rho(\mathbf{r}) = \begin{cases} 1, & 0 \le r \le 2a|cos\theta| \\ 0 & \text{otherwise} \end{cases}. \quad \text{(S3)}$$

Substituting this density into Eq. S2, we obtain

$$A_{lm}(q) = \begin{cases} (-1)^n 2\sqrt{2(4n+1)} \int_0^1 dx P_{2n}(x) \int_0^{2ax} drr^2 j_{2n}(qr), & l = 2n \text{ and } m = 0 \\ 0, & l = 2n+1 \text{ or } m \neq 0 \end{cases}, \quad \text{(S4)}$$

where $P_{2n}(x)$ are Legendre polynomials, and n is non-negative integer. Scattered intensity is

$$I(\mathbf{q}) = A(\mathbf{q})A^*(\mathbf{q}) = \frac{1}{4\pi}\sum_{l_1}\sum_{l_2}\sqrt{(2l_1+1)(2l_2+1)} A_{l_1 0}(q) A_{l_2 0}(q) P_{l_1}(cos\theta)\, P_{l_2}(cos\theta). \quad \text{(S5)}$$

Now partial scattered intensities can be found using product rule:

$$I_{l0}(q) = \sum_{l_1}\sum_{l_2}\sqrt{\frac{(2l_1+1)(2l_2+1)}{4\pi(2l+1)}}\, C(l_1 l_2 l; 000)^2 A_{l_1 0}(q) A_{l_2 0}(q), \quad \text{(S6)}$$

where $C(l_1 l_2 l; 000)$ are Clebsch-Gordan coefficients.

An equation, analogous to Eq. S2, relates partial scattered intensities $I_{l0}(q)$ to autocorrelation of electron density. Due to prefactor i^l the integral of $I_{l0}(q)$ over all q is positive for even $l/2$ (left column of Fig. 3), and

negative otherwise (right column of Fig. 3). This observation greatly simplifies checking for the correct sign assignment to $I_{l0}(q)$.

Supplementary Reference

30. Guinier, A. Diffraction of x-rays of very small angles-application to the study of ultramicroscopic phenomenon. *Annales de Physique* **12**, 161-237 (1939).